Magnetic phase diagrams and large magnetocaloric effects of the two-dimensional antiferromagnetic triangular lattice of Gd^{3+} ions in $KBaGd(BO_3)_2$

Z. M. Song,[1,*] N. Zhao,[1,*] H. Ge,[1] T. T. Li,[1] J. Yang,[2] L. Wang,[1,3] Y. Fu,[1] Y. Z. Zhang,[2] S. M. Wang,[1] J. W. Mei,[1,3,4] H. He,[5] S. Guo,[3,6] L. S. Wu,[1,4,7,†] and J. M. Sheng[1,8,‡]

[1]*Department of Physics, Southern University of Science and Technology, Shenzhen 518055, China*
[2]*Department of Chemsitry, Southern University of Science and Technology, Shenzhen 518055, China*
[3]*Shenzhen Institute for Quantum Science and Engineering, Southern University of Science and Technology, Shenzhen 518055, China*
[4]*Shenzhen Key Laboratory of Advanced Quantum Functional Materials and Devices, Southern University of Science and Technology, Shenzhen 518055, China*
[5]*School of Chemical Science, University of Chinese Academy of Sciences (UCAS), Beijing 100190, China*
[6]*International Quantum Academy, Shenzhen 518048, China*
[7]*Quantum Science Center of Guangdong-Hong Kong-Macao Greater Bay Area (Guangdong), Shenzhen 518045, China*
[8]*Academy for Advanced Interdisciplinary Studies, Southern University of Science and Technology, Shenzhen 518055, China*

(Received 23 June 2022; revised 14 February 2023; accepted 14 February 2023; published 13 March 2023)

We report a detailed study of the magnetic properties of $KBaGd(BO_3)_2$ in which magnetic Gd^{3+} ($S = 7/2$) ions form into two-dimensional triangular layers. Magnetization, specific heat, and magnetocaloric effect (MCE) measurements were performed on $KBaGd(BO_3)_2$ single crystals. The results show that a long-range antiferromagnetic state is established below $T_N = 0.24$ K. In zero fields, only about half of the full entropy is released at T_N, indicating that not all the magnetic moments are frozen below the ordering temperature, as expected from the geometrical frustration of the triangular spin lattice. Further studies under external fields were performed down to 50 mK and the magnetic phase diagrams are established with magnetic fields applied both within and perpendicular to the triangular plane. $KBaGd(BO_3)_2$ serves as an example of a two-dimensional triangular lattice with large spin values ($S = 7/2$) and can be directly compared with the isostructure $KBaR(BO_3)_2$ (R = Dy-Yb) family of doublet ground states, which exhibit effective spins of $S = 1/2$.

DOI: 10.1103/PhysRevB.107.125126

I. INTRODUCTION

Frustrated spin systems are one of the most attractive manifestations in demonstrating exotic collective phenomena in condensed matter physics [1–3]. Geometrical spin frustration arises when the system cannot realize a spin configuration where all the interactions are minimized simultaneously and thus cannot be stable at a unique ground state. As a consequence, strong quantum fluctuations are induced and macroscopic ground-state degeneracies with various exotic physics emerge at low temperatures [1,4–7]. As a prototype example of the realization of geometrical frustration, the triangular spin lattices with antiferromagnetic (AFM) exchange interactions have been well explored in the past [8–14]. Considering only the nearest-neighbor Heisenberg AFM exchange interactions, the magnetic ground state of the triangular spin lattice is proposed to be an ordered state of 120° spin configuration with a significantly reduced staggered moments due to the large quantum spin fluctuations [15–19].

Up to now, most studies on triangular lattices were focused on systems with spins $S = 1/2$ [13,14,20–22], where the quantum fluctuations are expected to be the greatest. In general, the strength of the quantum fluctuations will be reduced with larger values of S. However, experimental studies of the triangular spin lattices with different spin values are still relatively rare. The recently discovered rare-earth borate family compounds $KBaR(BO_3)_2$ with R = Y, Gd, Tb, Dy, Ho, Tm, Yb, and Lu, provided us a unique opportunity [23]. In this family of materials, the magnetic rare-earth ions form into perfect two-dimensional edge-shared triangular lattices, with the nonmagnetic potassium (K) and barium (Ba) ions stuffed in between. For rare-earth ions such as Yb, an effective $S = 1/2$ ground state is usually realized due to the crystalline electric field (CEF) splitting. On the other hand, the orbital contribution of Gd^{3+} is very small and a nearly isotropic $S = 7/2$ ground state is expected. Previous studies of $KBaGd(BO_3)_2$ reveal antiferromagnetic interactions between these magnetic Gd^{3+} ions based on the magnetization measurements [23]. In addition, no long-range magnetic order was found above 1.8 K [23]. It is still unclear whether the ground state is ordered below 1.8 K or whether a liquid or glass-like order is built up instead, as in the frustrated gadolinium garnet system $Gd_3Ga_5O_{12}$ [24–27].

In this paper, we perform the low-temperature magnetization and specific heat measurements on $KBaGd(BO_3)_2$ single crystals. Long-range magnetic order is observed at $T_N = 0.24$ K in zero field. In addition, this order is

*These authors contributed equally to this work.
†wuls@sustech.edu.cn
‡shengjm@sustech.edu.cn

TABLE I. Refined parameters and crystallographic data of $KBaGd(BO_3)_2$ from single crystal x-ray diffraction pattern.

Chemical formula	$KBaGd(BO_3)_2$
Formula weight	451.295
Temperature(K)	100
λ(Å)	0.71073
Crystal system	Trigonal
Space group, Z	$R\bar{3}m$(No.166), 3
a(Å)	5.4638(2)
b(Å)	5.4638(2)
c(Å)	17.9461(3)
α(°)	90
β(°)	90
γ(°)	120
V(Å^3)	464.0
ρ_{calc}(g/cm^3)	4.85
Goodness-of-fit	3.28
R_1	5.54
wR_2	6.12

gradually suppressed with the application of a magnetic field both along and perpendicular to the triangular lattice. No fractional plateau-like phases are induced in magnetic fields in either direction. On the other hand, only half of the full entropy is released at the transition temperature, indicating that a large amount of fluctuations persist above the transition temperature.

II. EXPERIMENTAL DETAILS

Single crystals of $KBaGd(BO_3)_2$ were synthesized, following the flux method reported in [23]. Pure raw materials of K_2CO_3, $BaCO_3$, and Gd_2O_3 were mixed with the stoichiometric ratio, while additional H_3BO_3 and KF were used as flux. All these precursors were placed in a platinum crucible. The temperature profile as described in [23] was used and transparent plate-like single crystals of $KBaGd(BO_3)_2$ with sizes about $1 \times 1 \times 0.5$ mm^3 were obtained after removing the left flux with distilled water.

The crystal structure and orientations of $KBaGd(BO_3)_2$ were verified using a Bruker D8 Quest diffractometer with Mo-Kα radiation ($\lambda = 0.71073$ Å). All the thermal property measurements were performed on single crystals, using the commercial Quantum Design Physical Property Measurement System (PPMS) and Magnetic Property Measurement System (MPMS).

III. RESULTS AND ANALYSIS

A. Crystal structure

$KBaGd(BO_3)_2$ crystallized in the hexagonal structure with the space group $R\bar{3}m$ [Fig. 1(a)]. The single crystal structure was verified at 100 K by the single crystal x-ray diffractometer, and the details of the refinement are given in Tables I and II. The refined lattice parameters are found out to be $a = b = 5.4638(2)$ Å, $c = 17.9461(3)$ Å with $\alpha = \beta = 90^o$ and $\gamma = 120^o$, which are consistent with previous reports [23]. In $KBaGd(BO_3)_2$, the magnetic Gd^{3+} ions form into an ideal

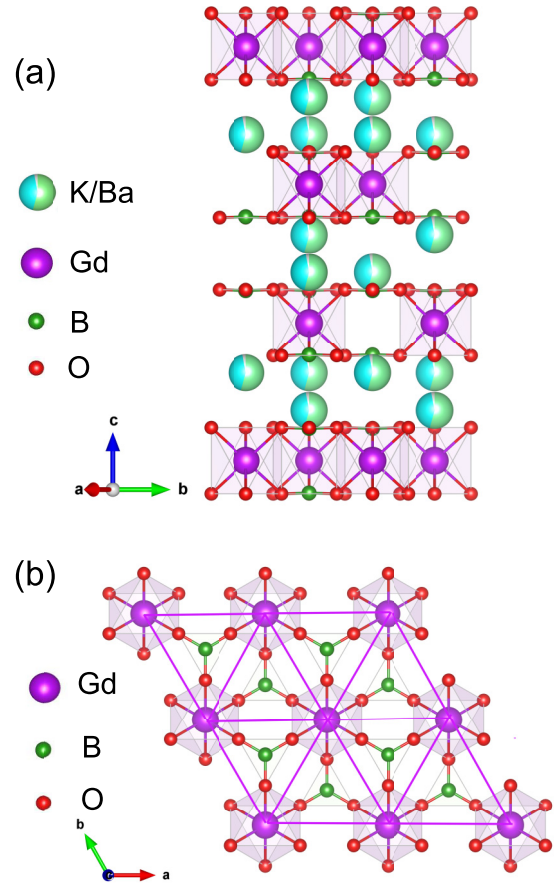

FIG. 1. (a) The crystal structure of $KBaGd(BO_3)_2$, where Gd^{3+} ions form into a perfect triangular layer in the ab plane and these triangular layers are stacked along the c axis. (b) Top view of the triangular layer of GdO_6 octahedra.

triangular layer in the ab-plane, with the nearest-neighbor Gd-Gd distance about 5.4638 Å [Fig. 1(b)]. These magnetic layers are then stacked along the c axis, with an interlayer distance of about 5.982 Å. Nonmagnetic ions such as K^+ and Ba^{2+} are stuffed in between these two-dimensional Gd layers. Our single crystal x-ray refinement shows that these K^+ and Ba^{2+} ions share the same crystallographic site ($6c$), and are randomly distributed with a ratio close to $0.510(5) : 0.495(5) \approx 1 : 1$ (Table II). Similar site disorder effects are also found in the isostructural compounds $KBaR(BO_3)_2$, where R = Y, Gd, Tb, Dy, Ho, Tm, Yb, and Lu [23,28].

The site disorder impact on the magnetic properties of these rare-earth ions are still under debate. Similar situations were found in the rare-earth triangular lattice magnet

TABLE II. Atomic displacement parameters of $KBaGd(BO_3)_2$.

Atom	Wkf.	x	y	z	Occupancy	U_{eq}
Ba	$6c$	0	0	0.7877(3)	0.510(5)	0.015(7)
K	$6c$	0	0	0.7876(9)	0.495(5)	0.015(9)
Gd	$3a$	0	0	0	1	0.009(4)
B	$6c$	0	0	0.590(6)	1	0.010(8)
O	$18h$	0.291(2)	0.145(9)	0.413(1)	1	0.015(6)

$YbMgGaO_4$ [22,29], where site disorder was found between the nonmagnetic Mg^{2+} and Ga^{3+} ions. Continuum-like spin excitations were observed in the inelastic neutron scattering experiments [11,30]. Based on this, spin-liquid ground states with spinon Fermi surfaces were proposed [11,31]. However, it was also argued that the effects of disorder play a more important role [32,33]. For the rare-earth elements with $L \neq 0$, the ground states are determined by the local charge environments due to the CEF splitting. The presence of the site disorder with different charges leads to distinct ground states on different sites. Thus, the intrinsic properties of $YbMgGaO_4$ might be affected by the disorder of the Mg^{2+} and Ga^{3+} ions. Unlike Yb^{3+} ions, Gd^{3+} ions of the ground state of ${}^8S_{7/2}$ ($S = 7/2, L = 0$) have much smaller orbital contributions. Weak single-ion anisotropy may arise from the mixing of the higher-level states at low temperatures [34,35]. Even with this considered, the CEF effect of Gd^{3+} and the orbital contribution are still much weaker than other rare-earth ions. Thus, the influence of the disorder of K^+ and Ba^{2+} ions is minimized in $KBaGd(BO_3)_2$.

In addition, the distances between the magnetic rare-earth ions in the borate family $KBaR(BO_3)_2$ are in the range of about 5–6 Å. This usually results in very weak spin correlations. However, due to the large spin value $S = 7/2$, the exchange interactions for Gd^{3+} ions are greatly enhanced, as compared to other family compounds such as $KBaYb(BO_3)_2$ [36,37].

B. Magnetization and phase diagram

The temperature-dependent dc magnetic susceptibility $\chi(T)$ with field applied in the *ab*-plane and *c* axis was measured, as shown in Fig. 2(a). A weak anisotropy is observed for the temperature range 2–300 K, and no sign of long-range magnetic order is observed for both directions above 2 K. The blue and red solid lines in Fig. 2(a) are the fits of the inverse magnetic susceptibility to the Curie-Weiss law $\chi = C/(T - \theta_{CW})$, where θ_{CW} is the Curie-Weiss temperature and C is a constant associated with the effective magnetic moment. The obtained Curie-Weiss temperatures are $\theta_{CW}^{ab} = -1.1 \pm 0.2$ K and $\theta_{CW}^{c} = -1.3 \pm 0.2$ K and the effective magnetic moments are $\mu_{eff}^{ab} = 7.9\ \mu_B$ and $\mu_{eff}^{c} = 7.8\ \mu_B$, for both field directions, respectively. These negative Curie-Weiss temperatures indicate weak antiferromagnetic exchange interactions in $KBaGd(BO_3)_2$, similar to the observations in [23].

Isothermal magnetization M(B) was measured at 2 K as presented in Fig. 2(b). The measured saturation moments are about 7 μ_B/Gd, for both field directions $B \parallel ab$ and $B \parallel c$. This is as expected for a free ion with $S = 7/2$. However, for magnetic fields below 4 T, a slightly anisotropic behavior is observed. The measured magnetization in the *ab*-plane is larger than the magnetization along the *c* axis, indicating a weak easy plane anisotropy. These observations are consistent with the previous studies [23]. However, to explore the effect of the geometrical frustration, characterizations at lower temperatures are needed.

To further investigate the ground state, magnetization measurements down to very low temperatures were performed, using a home-built Hall sensor magnetometer integrated with the dilution refrigerator probe [38–40]. For field in the *ab*-plane, the (110) direction (or $B \parallel b^*$) perpendicular to the hexagonal crystal edge was chosen. The isothermal magnetization $M(B)$ curves measured at different temperatures are presented in Figs. 3(a) and 3(b), respectively. When the measurement temperatures are well above the ordering temperature $T_N = 0.24$ K, the field-dependent magnetization follows the Brillouin function [insets of Figs. 3(a) and 3(b)]. Upon lowering the temperature, these magnetization data start to deviate from the paramagnetic behavior. As evidenced by the field derivative magnetic susceptibility dM/dB, sharp peaks built up as the temperature is reduced below T_N [Figs. 3(c) and 3(d)]. Finally, two peak-like anomalies are observed at about 0.03 T and 0.24 T, at 60 mK for $B \parallel b^*$. The magnetic phase diagram for $B \parallel b^*$ is summarized in Fig. 3(e). The intensity of the contour plot corresponds to the values of dM/dB. This phase diagram is similar to the observations in the Gd-based perovskites, such as $GdAlO_3$ [41] and $GdScO_3$ [42]. With only the nearest-neighbor interactions considered,

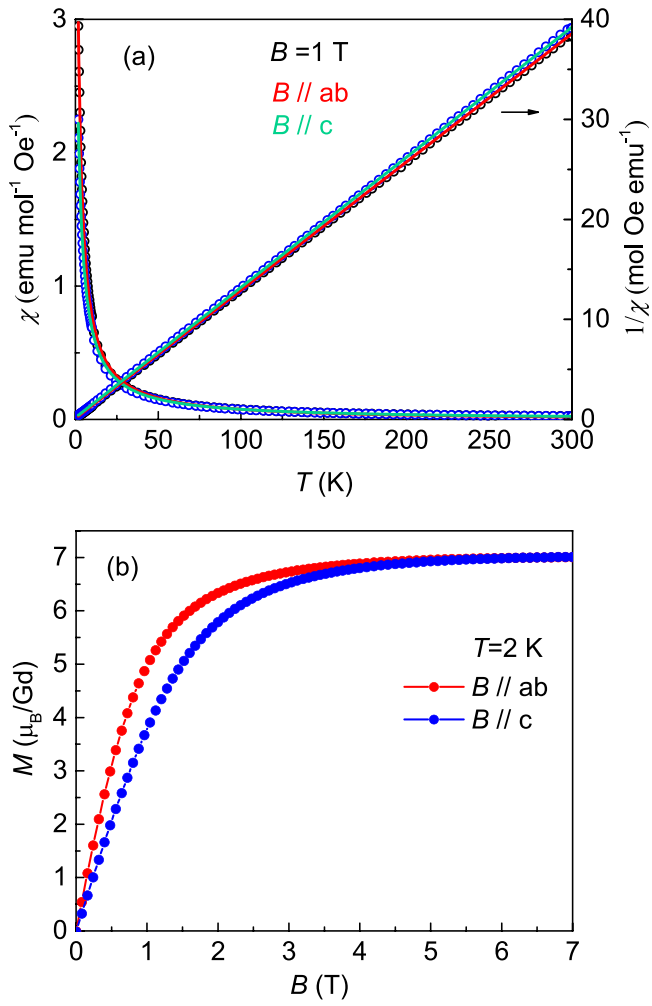

FIG. 2. (a) Temperature dependence of the magnetic susceptibility χ (left axis) and the inverse magnetic susceptibility $1/\chi$ (right axis) with the magnetic field parallel to the *ab* plane and *c* axis from 2–300 K. The blue and red solid lines indicate a Curie-Weiss fit to the inverse magnetic susceptibility over the entire temperature range. (b) Isothermal magnetization M(B) measured at 2 K with the magnetic field applied in the *ab* plane and *c* axis.

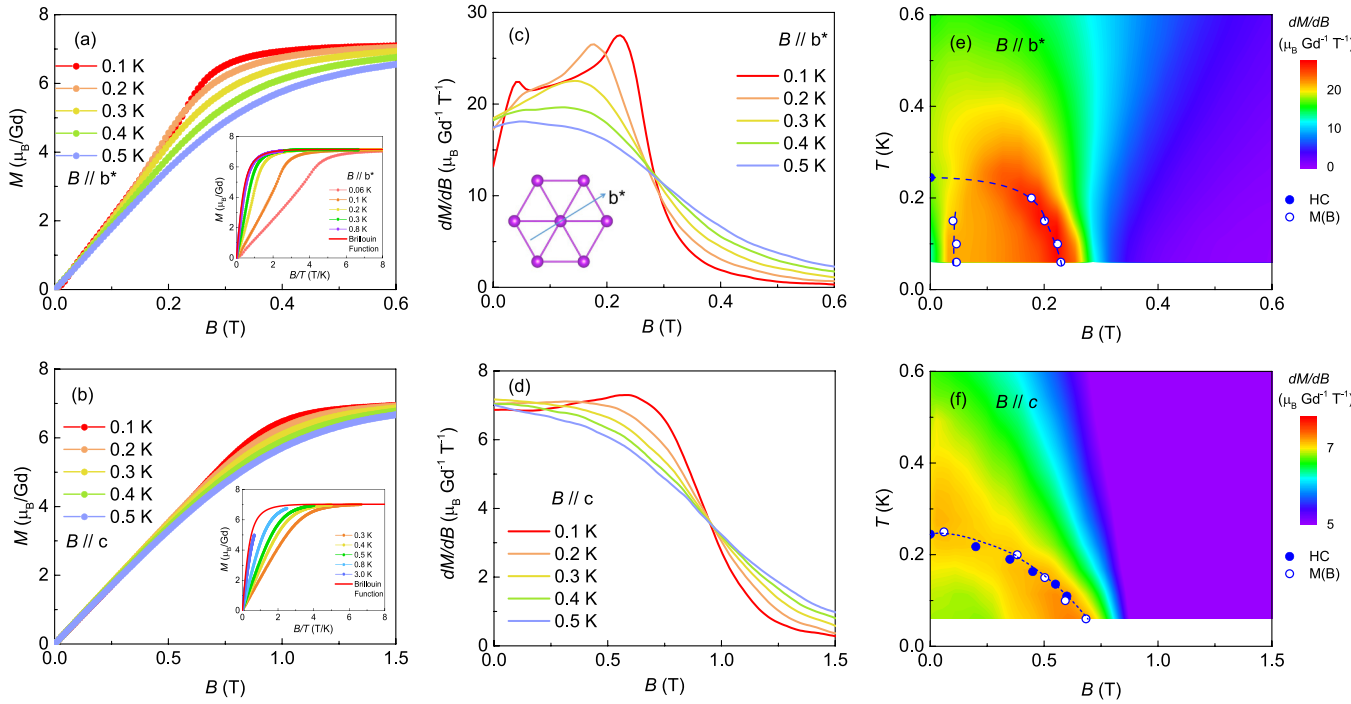

FIG. 3. (a,b) The field-dependent magnetization M measured at different temperatures in b^* and c directions, respectively. Insets: Comparison of the the measured magnetization and the simulated Brillouin function of $S = 7/2$. (c,d) The field derivative magnetic susceptibility dM/dB at different temperatures in b^* and c directions, respectively. (e,f) The field-temperature magnetic phase diagram overlaid on the contour plots of magnetic susceptibility dM/dB with field along the b^* and c directions, respectively.

the magnetic ground state of the easy plane triangular system was proposed to be a long-range-ordered phase with spins oriented 120° to each other. For $B \parallel b^*$, the zero field 120° order is destroyed with increasing field and spin flop-like transitions separate the magnetic phase diagram into two different regions. In the end, above the upper critical field at 0.24 T, all the Gd spins are fully polarized along the magnetic field.

On the contrary, for $B \parallel c$ only a single peak in dM/dB is observed for a field around 0.7 T at 0.06 K. The magnetic phase diagram for the field along c is presented in Fig. 3(f). In this case, the magnetic field is applied perpendicular to the Gd moments. The 120° ordered spins form a canted "V"-shaped phase, before fully polarizing along the c-axis. Since this is the hard direction, a larger saturation field is needed, compared to the saturation field 0.24 T for $B \parallel b^*$. It is worth pointing out that isotropic behavior is expected if only the ground state $^8S_{7/2}$ with $L = 0$ are considered. However, for Gd^{3+} ions, it was found that the mixing of the higher-level states of $L \neq 0$ cannot be neglected, especially for the physics at energy levels around 1–2 K [34,35,43]. This could be the origin of the easy plane anisotropy observed in $KBaGd(BO_3)_2$. To clarify the single ion anisotropy, further studies such as electron spin resonance (ESR) measurements are still needed in the future.

C. Specific heat, magnetic entropy, and magnetocaloric effect

Specific heat measurements were performed as well. Shown in Fig. 4(a) is the temperature-dependent specific heat measured in zero field. A λ-shaped peak centered at $T_N = 0.24$ K is observed. This indicates the establishment of a long-range magnetic order. However, unlike other traditional magnets, a long tail extending to about 2 K is observed in the specific heat, which is about eight times higher than the transition temperature $T_N = 0.24$ K. As also evidenced in the integrated magnetic entropy, only half of the full entropy ($0.47R\ln 8$) is released at $T_N = 0.24$ K and the full value of $R\ln 8$ as expected for spins of $S = 7/2$ is realized above 2 K. To account for the contribution below 70 mK, an estimated residual entropy with $S_0 \simeq 0.09R\ln 8$ is added. These results are in contrast to the observations found in classical Gd-based magnets, such as $GdAlO_3$ [44]. In the case of $GdAlO_3$, almost the full entropy of $R\ln 8$ was found at the transition temperature and only very weak contribution was left above the transition temperature. On the other hand, phenomena similar to what we find here were commonly observed in low-dimensional quantum magnets [45], where large spin fluctuations are usually present.

Additional specific heat under field has been measured and shown in Fig. 4. Due to the thin flat plate-shaped crystal geometry, only data with field along the c-axis were collected. From these temperature-dependent specific heat measured at different magnetic fields, it is noticed that the peak positions, together with the peak values in specific heat, are gradually suppressed with increasing fields [Fig. 4(c)]. As evidenced in the integrated entropy [Fig. 4(d)], only about $0.3R\ln 8$ is released at T_N at 0.5 T. All these phenomena indicate that a short-range order persists in a wide temperature region above the transition temperature. This indicates that the presence of the spin frustrations in this two-dimensional triangular layer plays an important role.

Moreover, the antiferromagnetic transition is fully suppressed at the critical field at $B_c \simeq 0.75$ T. In the meantime,

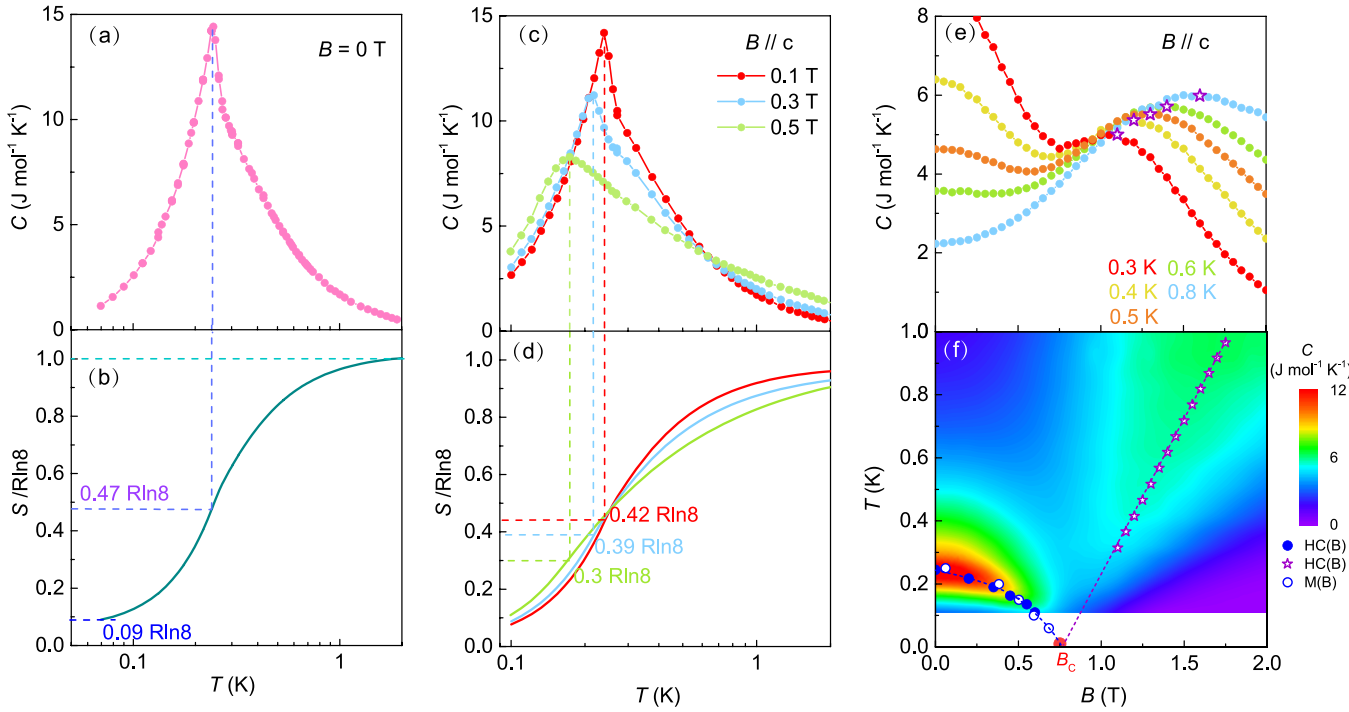

FIG. 4. (a) The temperature dependence of the specific heat C measured in zero fields. (b) The integrated magnetic entropy S as the function of temperature. The vertical dashed line indicates the magnetic transition temperature $T_N = 0.24$ K. (c) The temperature dependence of the specific heat below the critical field along c axis. (d) The temperature dependence of magnetic entropy below the critical field. (e) The field dependence of specific heat at different temperatures measured above the saturation fields along the c axis. (f) The field-temperature magnetic phase diagram overlaid on the contour plots of specific heat in c axis.

the measured specific heat monotonically increases with lower temperature [blue dots in Fig. 4(e)], suggesting that a significant residual entropy is pushed to zero temperature. As we continue to increase the field above B_c, a broad peak-like anomaly is observed at higher temperatures [purple dots in Fig. 4(e)]. In addition, these peak positions [indicated as stars in Fig. 4(e)] consistently move to higher temperatures with increasing fields. We have overplot all these specific heat data together with the magnetic phase diagram [Fig. 4(f)]. It is noticed that these peak positions extend linearly to the critical field B_c, indicating a gapless quantum critical point. These crossover-like behaviors above B_c are usually related to a gap reopening beyond the critical field. Interestingly, these crossover temperatures usually scale with the power law $T* \propto (B - B_c)^{\nu z}$, and the linearity suggests a two-dimensional universality of $\nu z = 1$, similar to the recent observations found in the triangular $S = 1/2$ system $Na_2BaCo(PO_4)_2$ [14].

Presented in Figs. 5(a) and 5(b) are the specific heat and the integrated entropy at 0.75 T and 2 T. The measured specific heat at 0.75 T keeps increasing as $T \to 0$, indicating a large enhancement of the zero-temperature residual entropy at the field-induced critical point. Due to the large relaxation time, the specific heat below 0.2 K at at 0.75 T was hard to measure. The residual entropy was estimated to be about $0.2R\ln 8$ by linearly extracting the specific heat C/T to zero as approaching 0 K. Meanwhile, the specific heat at low temperatures was greatly suppressed at 2 T, above the critical fields. This large entropy change near the critical region can be used for adiabatic demagnetization refrigeration [46]. As illustrated in Fig. 5(b) (blue dashed lines), a significant temperature drop ΔT can be expected by lowering the magnetic field from 2 T to 0.75 T due to the entropy change ΔS. To test this scenario, magnetocaloric effect (MCE) measurements were performed on a single crystal of the mass about 0.1 mg with $B \parallel c$. As the external fields were swept up and down, the sample temperatures were simultaneously recorded [Figs. 5(c) and 5(d)]. Instead of a sharp V-shaped anomaly, a rounded minimum-like feature was observed around the phase boundary. This is due to a small heat leakage from the environment and the sample is not in an ideal adiabatic condition. To achieve temperatures below 50 mK, measurements with larger crystals and better-designed MCE pucks are required in the future. However, even with the current setup using such a tiny crystal, we can still see a great magnetocaloric effect with a large magnetic Grüneisen parameter $\Gamma_B = 1/T(dT/dB)$ at the critical point [Fig. 5(c)]. The amplitude of the magnetic Grüneisen parameter Γ_B increases with decreasing temperature near the critical region [Fig. 5(c)]. This behavior is quite different from those systems where only weak fluctuations persist. In this case, the MCE curve becomes almost flat and the amplitude of the magnetic Grüneisen parameter drops to zero as the temperature was suppressed to zero [47]. The enhanced MCE effect in $KBaGd(BO_3)_2$ makes it a distinct promising candidate for adiabatic demagnetization cooling below 100 mK. In addition, due to the large magnetic entropy arising from the large spin value $S = 7/2$, the demagnetization cooling of $KBaGd(BO_3)_2$ at the critical field will be more efficient comparared to other $S = 1/2$ based materials.

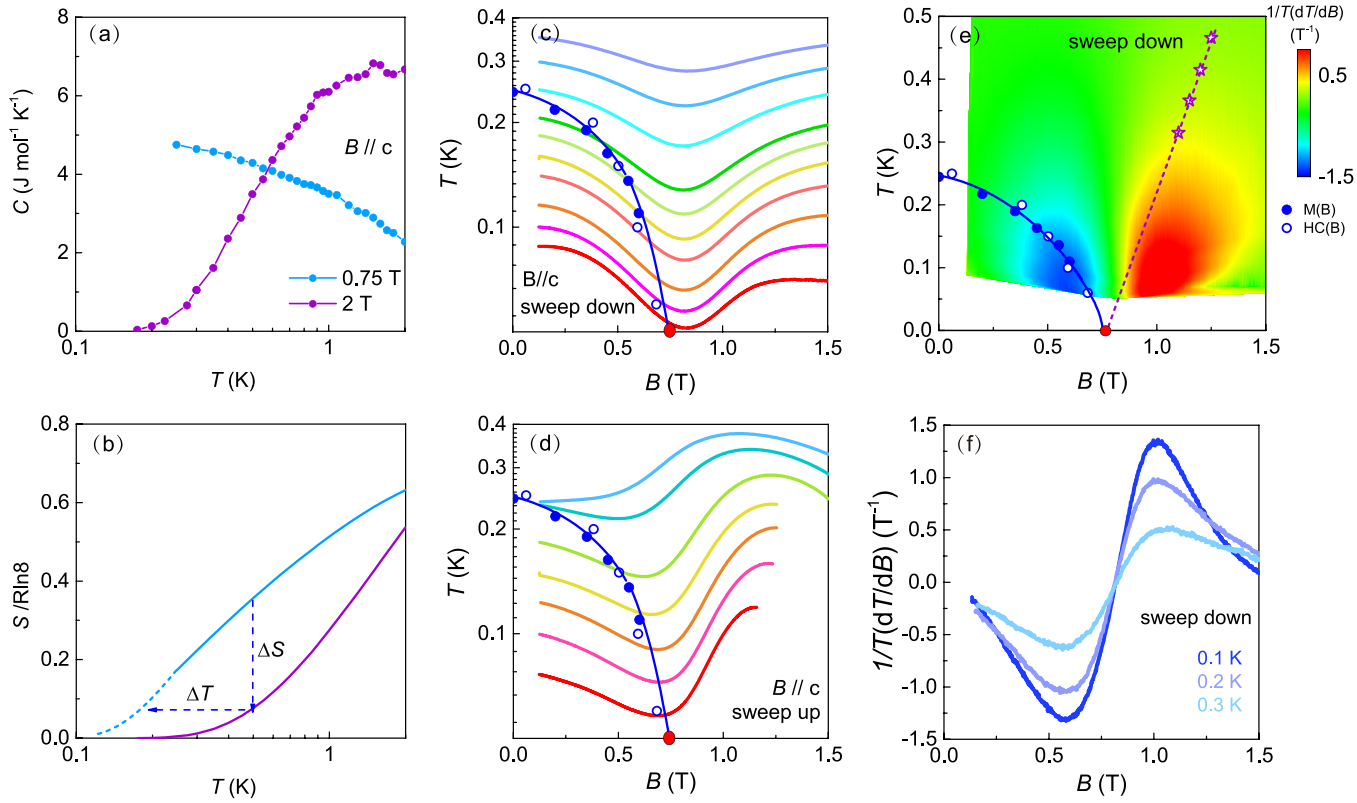

FIG. 5. (a) The temperature dependence of the specific heat at and above the critical field along the c axis. (b) The temperature dependence of the magnetic entropy at and above the critical field. Magnetocaloric effect of $KBaGd(BO_3)_2$ with the application of a magnetic field (c) sweep down and (d) sweep up. (e) The contour plot of magnetic Grüneisen parameter $\Gamma_B = 1/T(dT/dB)$. (f) The magnetic Grüneisen parameter Γ_B as a function of magnetic field at several temperatures.

IV. CONCLUSION

To summarize, detailed investigations with low-temperature magnetization, and specific heat were performed on $KBaGd(BO_3)_2$ single crystals. The magnetic Gd^{3+} ions form into a two-dimensional triangular lattice with a large spin $S = 7/2$. As the temperature is lowered, a long-range magnetic order is established below $T_N = 0.24$ K. To explore this ordered ground state, magnetic fields were applied in the triangular plane and along the c-axis. Although isotropic single ion properties are expected, the resulting magnetic phase diagrams are different from each other. The differences in the two phase diagrams arise from the weak easy-plan anisotropy, and they are consistent with the 120° spin order in the plane. Thus, for field applied along the b^* axis ($B \parallel (110)$), spin flop-like transitions with two successive critical fields are observed. While for field perpendicular to the magnetic moments with $B \parallel c$, the spins continuously rotated from the original (110) directions, until they are fully polarized along the c axis at the saturation field. Although the large spin values of Gd^{3+} ions do not make them as quantum as spin $S = 1/2$, wide temperature regions of short-range spin correlations are observed above the transition temperature, as evidenced by the specific heat and integrated magnetic entropy. This suggests that, even for the spin magnitude as large as 7/2, the zero point fluctuations proportional to $1/S$ still play an important role as $T \to 0$. On the other hand, these enhanced spin fluctuations and the large residual magnetic entropy hosted in $KBaGd(BO_3)_2$ can be utilized to realize efficient magnetic refrigeration in a moderate field region.

ACKNOWLEDGMENTS

The research at SUSTech was supported by the National Key Research and Development Program of China (Grant No. 2021YFA1400400), the National Natural Science Foundation of China (Grants No. 12134020, No. 11974157, No. 12174175, and No. 12104255), the Guangdong Basic and Applied Basic Research Foundation (Grant No. 2021B1515120015), the Shenzhen Fundamental Research Program (Grant No. JCYJ20220818100405013), the Science, Technology and Innovation Commission of Shenzhen Municipality (Grant No. ZDSYS20190902092905285). The Major Science and Technology Infrastructure Project of Material Genome Big-science Facilities Platform was supported by Municipal Development and Reform Commission of Shenzhen.

[1] A. P. Ramirez, Strongly geometrically frustrated magnets, Annu. Rev. Mater. Sci. **24**, 453 (1994).

[2] R. Moessner and A. P. Ramirez, Geometrical frustration, Phys. Today **59**(2), 24 (2006).

[3] L. Balents, Spin liquids in frustrated magnets, Nature (London) **464**, 199 (2010).

[4] M. J. Harris, S. T. Bramwell, D. F. McMorrow, T. H. Zeiske, and K. W. Godfrey, Geometrical Frustration in the Ferromagnetic Pyrochlore $Ho_2Ti_2O_7$, Phys. Rev. Lett. **79**, 2554 (1997).

[5] T. H. Han, J. S. Helton, S. Y. Chu, D. G. Nocera, J. A. Rodriguez-Rivera, C. Broholm, and Y. S. Lee, Fractionalized excitations in the spin-liquid state of a kagome-lattice antiferromagnet, Nature (London) **492**, 406 (2012).

[6] V. Zapf, M. Jaime, and C. D. Batista, Bose-Einstein condensation in quantum magnets, Rev. Mod. Phys. **86**, 563 (2014).

[7] O. A. Starykh, Unusual ordered phases of highly frustrated magnets: a review, Rep. Prog. Phys. **78**, 052502 (2015).

[8] S. Miyashita, Magnetic properties of Ising-like Heisenberg antiferromagnets on the triangular lattice, J. Phys. Soc. Jpn. **55**, 3605 (1986).

[9] A. V. Chubukov and D. I. Golosov, Quantum theory of an antiferromagnet on a triangular lattice in a magnetic field, J. Phys.: Condens. Matter **3**, 69 (1991).

[10] S. Yamashita, Y. Nakazawa, M. Oguni, Y. Oshima, H. Nojiri, Y. Shimizu, K. Miyagawa, and K. Kanoda, Thermodynamic properties of a spin-1/2 spin-liquid state in a κ-type organic salt, Nat. Phys. **4**, 459 (2008).

[11] Y. Shen, Y. D. Li, H. L. Wo, Y. S. Li, S. D. Shen, B. Y. Pan, Q. S. Wang, H. C. Walker, P. Steffens, M. Boehm, Y. Q. Hao, D. L. Quintero-Castro, L. W. Harriger, M. D. Frontzek, L. J. Hao, S. Q. Meng, Q. M. Zhang, G. Chen, and J. Zhao, Evidence for a spinon Fermi surface in a triangular-lattice quantum-spin-liquid candidate, Nature (London) **540**, 7634 (2016).

[12] S. Ito, N. Kurita, H. Tanaka, S. Ohira-Kawamura, K. Nakajima, S. Itoh, K. Kuwahara, and K. Kakurai, Structure of the magneticexcitations in the spin-1/2 triangular-latticeHeisenberg antiferromagnet $Ba_3CoSb_2O_9$, Nat. Commun. **8**, 235 (2017).

[13] M. M. Bordelon, E. Kenney, C. X. Liu, T. Hogan, L. Posthuma, M. Kavand, Y. Q. Lyu, M. Sherwin, N. P. Butch, C. Brown, M. J. Graf, L. Balents, and S. D. Wilson, Field-tunable quantum disordered ground state in the triangular-lattice antiferromagnet $NaYbO_2$, Nat. Phys. **15**, 1058 (2019).

[14] J. M. Sheng, L. Wang, A. Candini, W. R. Jiang, L. L. Huang, B. Xi, J. Z. Zhao, H. Ge, N. Zhao, Y. Fu *et al.*, Two-dimensional quantum universality in the spin-1/2 triangular-lattice quantum antiferromagnet $Na_2BaCo(PO_4)_2$, Proc. Natl. Acad. Sci. **119**, e2211193119 (2022).

[15] D. A. Huse and V. Elser, Simple Variational Wave Functions for Two-Dimensional Heisenberg Spin-1/2 Antiferromagnets, Phys. Rev. Lett. **60**, 2531 (1988).

[16] Th. Jolicoeur and J. C. Le Guillou, Spin-wave results for the triangular Heisenberg antiferromagnet, Phys. Rev. B **40**, 2727 (1989).

[17] B. Bernu, P. Lecheminant, C. Lhuillier, and L. Pierre, Exact spectra, spin susceptibilities, and order parameter of the quantum Heisenberg antiferromagnet on the triangular lattice, Phys. Rev. B **50**, 10048 (1994).

[18] R. R. P. Singh and D. A. Huse, Three-Sublattice Order in Triangular-and Kagomé-Lattice Spin-Half Antiferromagnets, Phys. Rev. Lett. **68**, 1766 (1992).

[19] S. R. White and A. L. Chenyshev, Neél Order in Square and Triangular Lattice Heisenberg Models, Phys. Rev. Lett. **99**, 127004 (2007).

[20] R. Coldea, D. A. Tennant, A. M. Tsvelik, and Z. Tylczynski, Experimental Realization of a 2D Fractional Quantum Spin Liquid, Phys. Rev. Lett. **86**, 1335 (2001).

[21] Y. Shirata, H. Tanaka, A. Matsuo, and K. Kindo, Experimental Realization of a Spin-1/2 Triangular-Lattice Heisenberg Antiferromagnet, Phys. Rev. Lett. **108**, 057205 (2012).

[22] Y. S. Li, H. J. Liao, Z. Zhang, S. Y. Li, F. Jin, L. S. Ling, L. Zhang, Y. M. Zou, L. Pi, Z. R. Yang, J. F. Wang, Z. H. Wu, and Q. M. Zhang, Gapless quantum spin liquid ground state in the two-dimensional spin-1/2 triangular antiferromagnet $YbMgGaO_4$, Sci. Rep. **5**, 16419 (2015).

[23] S. Guo, T. Kong, F. A. Cevallos, K. Stolze, and R. J. Cava, Crystal growth, crystal structure and anisotropic magnetic properties of $KBaR(BO_3)_2$ (R= Y, Gd, Tb, Dy, Ho, Tm, Yb and Lu) triangular lattice materials, J. Magn. Magn. Mater. **472**, 104 (2019).

[24] O. A. Petrenko, C. Ritter, M. Yethiraj, and D. M. K. Paul, Spin-liquid behavior of the gadolinium gallium garnet, Physica B **241-243**, 727 (1997).

[25] O. A. Petrenko, C. Ritter, M. Yethiraj, and D. M. Paul, Investigation of the Low-Temperature Spin-Liquid Behavior of the Frustrated Magnet Gadolinium Gallium Garnet, Phys. Rev. Lett. **80**, 4570 (1998).

[26] O. A. Petrenko, D. M. Paul, C. Ritter, T. Zeiske, and M. Yethiraj, Magnetic frustration and order in gadolinium gallium garnet, Phys. B (Amsterdam, Neth.) **266**, 41 (1999).

[27] Y. K. Tsui, J. Snyder, and P. Schiffer, Thermodynamic study of excitations in a three-dimensional spin liquid, Phys. Rev. B **64**, 012412 (2001).

[28] M. B. Sanders, F. A. Cevallos, and R. J. Cava, Magnetism in the $KBaRE(BO_3)_2$(RE=Sm, Eu, Gd, Tb, Dy, Ho, Er, Tm, Yb, Lu) series: materials with a triangular rare earth lattice, Mater. Res. Express **4**, 036102 (2017).

[29] Y. S. Li, D. Adroja, R. I. Bewley, D. Voneshen, A. A. Tsirlin, P. Gegenwart, and Q. M. Zhang, Crystalline Electric-FieldRandomness in the Triangular Lattice Spin-Liquid $YbMgGaO_4$, Phys. Rev. Lett. **118**, 107202 (2017)

[30] J. A. M. Paddison, M. Daum, Z. Dun, G. Ehlers, Y. Liu, M. B. Stone, H. Zhou, and M. Mourigal, Continuous excitations of the triangular-lattice quantum spin liquid YbMgGaO4, Nat. Phys. **13**, 117 (2017).

[31] Y. D. Li, Y. M. Lu, and G. Chen, SpinonFermi surfaceU(1)spin liquid in the spin-orbit-coupled triangular-lattice MottinsulatorYbMgGaO$_4$, Phys. Rev. B **96**, 054445 (2017).

[32] Z. Ma, J. H. Wang, Z. Y. Dong, J. Zhang, S. C. Li, S. H. Zheng, Y. J. Yu, W. Wang, L. Q. Che, and K. J. Ran, Spin-Glass Ground State in a Triangular-Lattice Compound $YbZnGaO_4$, Phys. Rev. Lett. **120**, 087201 (2018).

[33] X. Rao, G. Hussain, Q. Huang, W. J. Chu, N. Li, X. Zhao, Z. Dun, E. S. Choi, T. Asaba, L. Chen *et al.*, Survival of itinerant excitations and quantum spin state transitions in $YbMgGaO_4$ with chemical disorder, Nat. Commun. **12**, 4949 (2021).

[34] V. N. Glazkov, M. E. Zhitomirsky, A. I. Smirnov, H.-A. Krug von Nidda, A. Loidl, C. Marin, and J.-P. Sanchez, Single-ion anisotropy in the gadolinium pyrochlores studied by electron paramagnetic resonance, Phys. Rev. B **72**, 020409(R) (2005).

[35] V. N. Glazkov, A. I. Smirnov, J. P. Sanchez, A. Forget, D. Colson, and P. Bonville, Electron spin resonance study of the single-ion anisotropy in the pyrochlore antiferromagnet $Gd_2Sn_2O_7$, J. Phys.: Condens. Matter **18**, 2285 (2006).

[36] B. L. Pan, J. M. Ni, L. P. He, Y. J. Yu, Y. Xu, and S. Y. Li, Specific heat and thermal conductivity of the triangular-lattice rare-earth material $KBaYb(BO_3)_2$ at ultralow temperature, Phys. Rev. B **103**, 104412 (2021).

[37] Y. Tokiwa, S. Bachus, K. Kavita, A. Jesche, A. A. Tsirlin, and P. Gegenwart, Frustrated magnet for adiabatic demagnetization cooling to milli-kelvin temperatures, Commun. Mater. **2**, 42 (2021).

[38] Magnetometry by means of Hall microprobes in the Quantum Design PPMS, Quantum Design Application Note, 1084-701.

[39] A. Cavallini, Deep levels in MBE grown AlGaAs/GaAs heterostructures, Microelectron. Eng. **73-74**, 954 (2004).

[40] A. Candini, G. C. Gazzadi, A. di Bona, M. Affronte, D. Ercolani, G. Biasiol, and L. Sorba, Hall nano-probes fabricated by focused ion beam, Nanotechnology **17**, 2105 (2006).

[41] K. W. Blazey and H. Rohrer, Antiferromagnetism and the magnetic phase diagram of $GdAlO_3$, Phys. Rev. **173**, 574 (1968).

[42] J. M. Sheng, X. C. Kan, H. Ge, P. Q. Yuan, L. Zhang, N. Zhao, Z. M. Song, Y. Y. Yao, J. N. Tang, S. M. Wang, M. L. Tian, X. Tong, and L. S. Wu, Low temperature magnetism in the rare-earth perovskite $GdScO_3$, Chin. Phys. B **29**, 057503 (2020).

[43] A. Ali Biswas and Y. M. Jana, Estimation of single-ion anisotropies, crystal-field and exchange interactions in gd-based frustrated pyrochlore anti-ferromagnets $Gd_2M_2O_7$ (M=Ti, Sn, Hf, Zr), J. Magn. Magn. Mater. **323**, 3202 (2011).

[44] S. Mahana, U. Manju, and D. Topwal, Giant magnetocaloric effect in $GdAlO_3$ and a comparative study with $GdMnO_3$, J. Phys. D: Appl. Phys. **50**, 035002 (2017).

[45] L. S. Wu, S. E. Nikitin, Z. Wang, W. Zhu, C. D. Batista, A. M. Tsvelik, A. M. Samarakoon, D. A. Tennant, M. Brando, L. Vasylechko *et al.*, Tomonaga luttinger liquid behavior and spinon confinement in $YbAlO_3$, Nat. Commun. **10**, 698 (2019).

[46] B. Wolf, Y. Tsuia, D. J. Nagara, U. Tutscha, A. Honeckerb, K. R. Langera, G. Hofmanna, A. Prokofievc, W. Assmusa, G. Donathd, and M. Langa, Magnetocaloric effect and magnetic cooling near a field-induced quantum-critical point, Proc. Natl. Acad. Sci. U.S.A. **108**, 6862 (2011).

[47] L. S. Wu, Y. Janssen, C. Marques, M. C. Bennett, M. S. Kim, K. Park, Songxue Chi, J. W. Lynn, G. Lorusso, G. Biasiol, and M. C. Aronson, Magnetic field tuning of antiferromagnetic Yb_3Pt_4, Phys. Rev. B **84**, 134409 (2011).